Earthq Eng & Eng Vib (2022) 21: 101-116 **DOI**: https://doi.org/10.1007/s11803-021-2068-x

Analyzing uncertainties involved in estimating collapse risk with and without considering uncertainty probability distribution parameters

Mohammad Amin Bayari[1†], Naser Shabakhty[2‡] and Esmaeel Izadi Zaman Abadi[1‡]

1. *Department of Civil Engineering, Najafabad Branch, Islamic Azad University, Najafabad 8514143131, Iran*

2. *School of Civil Engineering, Iran University of Science and Technology, Tehran 16844, Iran*

Abstract: In the present study, modified Ibarra, Medina and Krawinkler moment-rotation parameters are used for modeling the uncertainties in concrete moment frame structures. Correlations of model parameters in a component and between two structural components were considered to analyze these uncertainties. In the first step, the structural collapse responses were obtained by producing 281 samples for the uncertainties using the Latin hypercube sampling (LHS) method, considering the probability distribution of the uncertainties and performing incremental dynamic analyses. In the second step, 281 new samples were produced for the uncertainties by the central composite design (CCD) method without considering the probability distribution of the uncertainties and calculating the structural collapse responses. Then, using the response surface method (RSM) and artificial neural network (ANN) for the two simulation modes, structural collapse responses were predicted. The results indicated that the collapse responses at levels of 0 to 100% obtained from the two simulations have a high correlation coefficient of 98%. This suggests that random variables can be simulated without considering the probability distribution of uncertainties, by performing uncertainty analysis to determine structural collapse responses.

Keywords: uncertainty analysis; collapse response; artificial neural network; response surface method

1 Introduction

Sideway collapse, which is defined as a lateral instability of a structure due to strong ground motions, has been considered by researchers in recent years (Liel *et al.*, 2009; Zareian and Krawinkler, 2007; Zareian *et al.*, 2010). In this regard, identifying different uncertainty resources to predict collapse capacity and accurately describe the seismic performance of structures is of great importance (Ugurhan *et al.*, 2014). Two main uncertainty resources affect the collapse probability of structures; i.e., aleatory uncertainties resulting from the inherent nature of phenomena and epistemic uncertainties due to the lack of knowledge and inaccurate analytical models. In determining structural collapse probabilities, intensive motion features such as ground motion duration, earthquake frequency content, and earthquake intensity parameters are considered as aleatory uncertainties (record to record), while the assumptions made in the structural analysis are treated as epistemic uncertainties. Epistemic uncertainties can be reduced by developing scientific relations, collecting more data, and using a proper analytical model (Der Kiureghian and Ditlevsen, 2009). Due to the relatively limited knowledge of model parameters and collapse-related behavior, modeling uncertainties have received much attention in simulating the structural collapse response. They are needed to idealize nonlinear deformation demands and various sources of degradation both at the component and structure levels. Concentrated plastic hinge models are the best candidate for modeling structural collapse responses. Parameters employed to define concentrated plastic hinge models are typically calibrated by empirical relationships, which are a major source of uncertainties for structural collapse response simulation (Ugurhan *et al.*, 2014).

The incremental dynamic analysis (IDA) is introduced to consider the intrinsic variability effects of an earthquake in the seismic response analyses of structures. In this method, an earthquake record is scaled to cover a wide range of seismic intensities to consider uncertainties in seismic intensity prediction. Furthermore, to consider existing uncertainties in the frequency contents and spectral shapes of earthquakes, a considerable number of earthquake records are employed. This method is considered to predict the capacities of structures in the FEMA-350 Code (FEMA, 2000).

Simulation methods such as the Monte Carlo and the Latin hypercube sampling (LHS) are used

Correspondence to: Esmaeel Izadi Zaman Abadi, Department of Civil Engineering, Najafabad Branch, Islamic Azad University, Najafabad 8514143131, Iran
Tel: +98-9131653053
E-mail: e.izadi@pci.iaun.ac.ir
[†]PhD Candidate; [‡]Assistant Professor
Received August 26, 2019; **Accepted** March 9, 2020

to incorporate these uncertainties. A large number of simulations are required to cover the probability distribution of uncertainties, which is a time-consuming practice. To reduce computational efforts, the response surface method (RSM) is proposed in combination with simulation methods. In addition to RSM, alternative methods can be employed to consider uncertainties in prediction models, including artificial neural network (ANN) and neuro-fuzzy network (Beheshti-Aval *et al.*, 2015).

Vamvatsikos and Cornell (2004), Zareian and Krawinkler (2007) studied IDA-based methods to evaluate structural collapse. Ibarra and Krawinkler (2005) proposed a method to evaluate the global collapse of structures based on the relative intensity measure and engineering demand parameter. They defined global collapse as the inability of a structural system to resist gravity loads in the presence of seismic effects. The relative intensity increases until the system response becomes unstable; that is, the relative intensity-engineering demand parameter curve becomes flat. They named the largest relative intensity as the collapse capacity. Haselton *et al.* (2008) tested reinforced concrete columns to calibrate and determine the proper measures of the tri-linear model parameters proposed by Ibarra *et al*. (2005). Then, they proposed a set of empirical relationships for each parameter by conducting statistical studies and multivariate regression analysis. Lignos and Krawinkler (2010) proposed a database for modeling steel components based on the tri-linear model of Ibarra *et al*. (2005). Li (1996) demonstrated that any form of functions and its derivatives can be estimated using ANN, while the use of ANN creates lower prediction errors than RSM. Gomes and Miguel (2004) compared RSM and ANN in evaluating the reliability of a structure that had an implicit limit state function. They indicated that the use of these two methods to estimate the limit state function decreases the reliability of the evaluation when compared to the Monte Carlo method.

Bucher and Most (2008) compared response function methods and indicated that selecting the response function would be different depending on the problem. According to the examples of this study, response surface methods based on polynomial functions, radial basis functions (RBFs), and ANN have the ability to accurately consider failure conditions. Buratti *et al.* (2010) employed a parabolic model to estimate the structural response of a reinforced concrete moment frame considering uncertainties in structural features and ground motion parameters when an earthquake happens. They drew fragility curves according to the evaluated parabolic model. Park and Towashiraporn (2014) applied RMS for the probability evaluation and seismic vulnerability of steel bridges. They fitted the limit state function in the form of a second-order polynomial function by considering the uncertainties involved and not considering the interaction terms, calculating the probability of exceeding the damage states based on the fitted response surface functions. Khojastehfar *et al.* (2014) employed ANN and RSM in combination with the Monte Carlo method to develop collapse fragility curves by considering uncertainties in a steel moment frame. They showed that it is more accurate to determine the mean measures and standard deviations of the fragility curves by the ANN-based Monte Carlo simulation approach than by the RSM-based Monte Carlo method. Borekci *et al.* (2014) studied the collapse potential of SDOF systems caused by dynamic instability with stiffness and strength degradation. They introduced an equation to estimate the collapse period of SDOF systems as a function of the strength reduction factor, ductility level, and post-capping stiffness ratio. Investigating structural reliability requires a long computation time. In this regard, Gholizadeh and Mohammadi (2016) employed a wavelet back-propagation (WBP) neural network (NN) to predict the required deterministic and probabilistic structural nonlinear seismic responses at performance levels. Karimi and Şensoy (2016) used metaheuristic algorithms to evaluate the collapse responses of steel moment frames by considering different uncertainty sources. They adopted the IDA method to incorporate record-to-record uncertainties. The model uncertainties were applied by backbone curves and hysteresis loops. Also, cognitive uncertainties were provided at three levels of material quality. The analytical questions of the RSM were derived from the IDA results obtained using the Cuckoo algorithm, which predicts the means and standard deviations of collapse fragility curves. The Takagi-Sugeno-Kang model was employed to represent the material quality. Finally, collapse fragility curves with the uncertainties were obtained by various material quality values derived from the fuzzy Takagi-Sugeno-Kang model. The results indicated that better risk management strategies in countries with weak material quality control create cognitive uncertainties in fragility curves and the mean annual frequency. Zhang *et al.* (2017) introduced a novel approach, i.e., time-dependent reliability analysis with response surface (TRARS), to estimate the time-dependent reliability for nondeterministic structures under stochastic loads. They treated random variables and the maximum responses of uncertain structures as the input and output parameters, respectively. They also proposed a novel iterative procedure by introducing the response surface (RS) model. Moreover, they used a Butcher strategy to produce initial sample points while employing the gradient projection technique to produce new sample points to update the RS model in each iteration. Then, the time-dependent reliability indices and probabilities of failure were obtained using the first-order reliability method over a certain design lifetime. Karimi and Beheshti Aval (2018) applied adaptive neuro fuzzy inference system (ANFIS) models based on grid partition (GP), subtractive clustering (SC), and fuzzy C-means (FCM) to analyze uncertainties and predict seismic fragility curves of a steel moment frame. They

indicated that ANFIS-FCM predicts fragility curves more accurately than GP and SC methods. Gholizadeh and Aligholizadeh (2019) proposed a meta-model to reduce the computation burden of the Monte Carlo method in the optimization setting. The computation burden of a reliability-based optimal seismic design (RBOSD) is very high due to the huge number of nonlinear pushover analyses. To cope with this problem, they used a simple multilayer perceptron (MLP) model as an NN model to predict the necessary deterministic and probabilistic seismic responses during optimization. A meta-model composed of WPB was introduced for evaluating seismic responses. According to the FEMA-P695 Code (FEMA, 2009), the total system collapse uncertainties (β_{TOT}) are calculated by combining different uncertainty sources, including record-to-record (β_{RTR}), design requirements (β_{DR}), test data (β_{TD}), and modeling (β_{MDL}). Fattahi and Gholizadeh (2019), Hassanzadeh and Gholizadeh (2019) employed such uncertainties to determine the collapse margin ratio (CMR) for optimal structures, graphing the optimal structures′ fragility curves. Palanci (2019) introduced a risk assessment model for one-story precast industrial structures by fuzzy logic. Karimi and Şensoy (2020) adopted the optimized fuzzy method FCM-PSO to determine collapse fragility curves by considering the uncertainties. They revealed that this method is advantageous with regard to both accuracy and execution time in estimating the mean and standard deviation of fragility curves. In this study, the input, output, and relations of the fuzzy-based risk assessment model were determined by the reference buildings. The supervised learning method was used to determine the membership function of fuzzy sets and found that fuzzy logic is a promising technique for seismic assessment of structures and can be used as an effective instrument in rapid performance screening of the structures.

In the present study, two different methods of producing random samples and simulation with and without considering the probability distribution parameters of the uncertainties are employed to investigate the effects of uncertainties on structural collapse responses. The LHS method was used to generate samples with considering the probability distribution of the uncertainties, while the central composite design (CCD) was adopted to produce samples without considering the probability distribution of the uncertainties. Moreover, a combination of the above-mentioned simulation methods, RSM, and ANN was employed to predict risk and collapse fragility curves.

2 Model estimation and prediction methods

2.1 Artificial neural network (ANN)

Artificial neural network (ANN) is a method used to estimate functions and predict different systems. Such networks yield acceptable results when there are nonlinear relationships between the input and output of a system. Any network is made up of an input layer, an output layer, and one or more hidden layers. There are a number of neurons inside each of the layers that are connected by weighted connections (Fig. 1). During the network training, the weighs are continuously adjusted to minimize errors. To transfer the outputs of each layer to the next layers, purline, tansing, tangent hyperbolic and sigmoid functions are typically used.

An ANN structure is the multi-layer perceptron (MLP). An MLP can be trained using nonlinear functions such that it can estimate and predict any measurable function. Using a set of real input and output data, ANNs employ training algorithms to form hidden connections between input and output data through weight coefficients, biases, and the applied functions of each layer′s outputs. A portion of data (70%, for example) is typically used to train the network and the remaining portion is employed in data validation and network prediction tests.Various training algorithms have been employed to train ANNs, one of the most important of which being error back propagation algorithm (Anderson, 1995).

2.2 Response surface method (RSM)

In this study, the CCD is used to design the model. CCD includes a full factorial design or two-stage fractional factorial design with axial and central points. Using such designs, the curve of a system can be estimated. The design is performed based on three levels of factorial points, axial points, and central points, (Fig. 2).

The number of experiments in CCD is calculated as Eq. (1)

$$N = 2^{k-p} + (2k+1) + n_c \tag{1}$$

where N is the number of experiments, k is the number of variables, p is a fraction of full factorial design, and n_c is the number of replications. The three terms in Eq. (1) denote factorial points, star points (including axial and central points), and the number of replications, respectively. Figure 3 shows CCD for three factors.

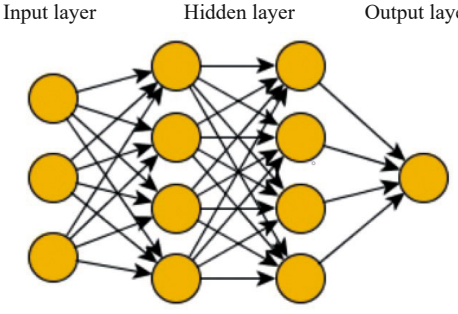

Fig. 1 Structure of a multi-layered perceptron (MLP)

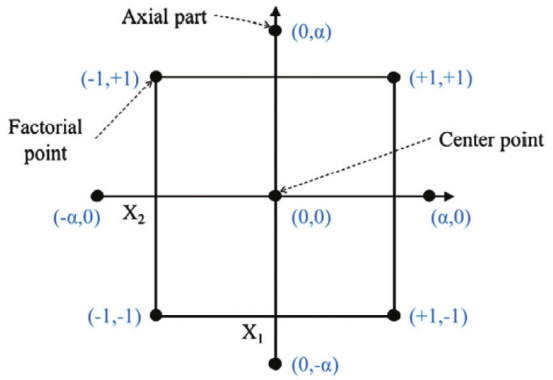

Fig. 2 Factorial, central, and axial points in CCD

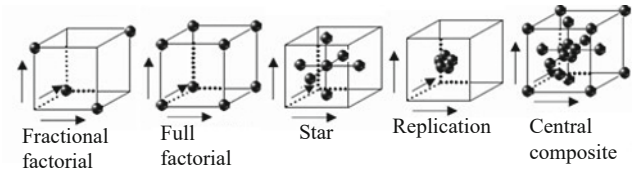

Fig. 3 CCD for three factors

CCD provides a quadratic equation as Eq. (2)

$$y = \beta_0 + \sum_{i=1}^{k} \beta_i x_i + \sum_{i=1}^{k} \beta_{ii} x_i^2 + \sum_{i=1}^{k} \sum_{j=1}^{k} \beta_{ij} x_i x_j + \varepsilon \qquad (2)$$

where β_0, β_i, β_{ii} and β_{ij} are the constant, linear, quadratic, and interaction coefficients of the factors, respectively. x_i and x_j are independent coded variables. Equation (2) is a polynomial regression model. The unknown polynomial coefficients are calculated by minimizing the sum of squares of residuals (i.e., the difference between the observed values and estimated function values) (Myers *et al.*, 2009).

3 Structural dynamic analysis

3.1 Dynamic analysis of structure

Incremental dynamic analysis (IDA) is a method to determine the fragility curves of structures′ limit states under different seismic intensities. To perform IDA, proper parameters must be selected to reflect the intensity measure (IM) and demand measure (DM). A proper IM selection leads to lower dispersion in the structure′s response to various earthquakes and thus more accurate estimation of the responses′ statistical measures. In the present study, IM was considered to be the spectral acceleration in the fundamental period of the structure ($S_a(T_1)$). DM is a parameter selected to make the best structural response reflection, which was considered to be the maximum inter-story drift in this study; i.e., maximum among the floors and during the total earthquake time. For IDA analysis, earthquake records were selected and each record was scaled to a small measure of IM that produced linear behavior in the structure′s model, under which time history analysis became nonlinear. The process of scaling IM continues on a proper algorithm until the structural collapse limit is obtained. For the incremental trend of IDA, it is required to select IM values using a proper algorithm to optimize the number of analysis points such that the minimum number of points in the initial linear areas and the maximum number of points in the collapse-prone areas are selected to achieve sufficient accuracy. As a result, the distances between consecutive IMs for each earthquake record can be determined in proportion to its collapse level. The algorithm used in this study for IDA was adapted from the Hunt-Fill algorithm (Vamvatsikos and Cornell, 2002).

After completing each IDA stage, the IM variations were plotted versus the DM of the record.

3.2 Structural collapse criteria

From an engineering perspective, collapse occurs when the lateral drifts of one or more floors becomes larger than the other floors such that the structural system is no longer able to resist the gravity loads due to the secondary moment induced by the building′s weight (P-Delta effect). Thus, according to FEMA-350 Code (FEMA, 2000), IDA can be employed to estimate the structural collapse capacity. According to the code′s recommendation, the collapse point is considered to be equal to the occurrence of one of the following:

- Numerical non-convergence in the structural analysis algorithm;
- A slope of 20% of the initial elastic slope in the IDA curve; and
- Maximum inter-story drift exceeding 0.1.

It was observed in many cases that the determination of structural collapse based on the non-convergence criterion or the minimum slope contradicts real observations and engineering experience in terms of θ_{max} created in the structure. To handle this problem, structural collapse is simultaneously controlled by two criteria of minimum slope and $0.1 \leq \theta_{max}$.

According to the earthquake intensity method, collapse limit state refers to an intensity of earthquake that collapses the structure. In other words, IM_{cap} or $IM_{collapse}$ represents the last point of seismic intensity on the IDA curve under which the structure does not collapse. After IM_{cap}, the IDA curve slope falls below 20% of the elastic slope or the inter-story drift exceeds 0.1.

For each IDA curve, there is a point with a seismic intensity corresponding to collapse that is denoted by $IM_{collaps}$. The possible curve of fitting the mentioned points on several IDA curves represent collapse fragility curves, which are defined as Eq. (3) (Tothong and Cornell, 2007):

$$P_{C|IM=im} = \phi\left(\frac{\ln im - \mu_{\ln IM_{cap}}}{\sigma_{\ln IM_{cap}}}\right) \qquad (3)$$

where $\mu_{\ln IM_{cap}}$ and $\sigma_{\ln IM_{cap}}$ denote the mean and standard deviation of collapse based on IM and are defined as Eqs. (4) and (5), respectively.

$$\mu_{\ln IM_{cap}} = \frac{1}{n}\sum_{i=1}^{n} \ln im_{cap,i} \tag{4}$$

$$\sigma_{\ln IM_{cap}} = \sqrt{\frac{\sum_{i=1}^{n} (\ln im_{cap,i} - \mu_{\ln IM_{cap}})^2}{n-1}} \tag{5}$$

where $im_{cap,i}$ is the IM_{cap} value of record i, and n is the number of records.

3.3 Probabilistic seismic demand analysis (PSDA)

Probabilistic seismic demand analysis (PSDA) is a good method to calculate the mean annual frequency (MAF) of exceedance of various given values.

PSDA integrates the site-specific seismic hazard curve (e.g., spectral acceleration hazard curve) calculated by probabilistic seismic hazard analysis (PSHA) with the nonlinear dynamic analysis results of the structure collected using a set of accelerograms.

The mean annual frequency (MAF) of exceedance of a given limit state, i.e., λ_{LS}, is calculated as Eq. (6)

$$\lambda_{LS} = \int G_{LS|DM}(y) \cdot \left| d\lambda_{DM}(y) \right| \tag{6}$$

where $d\lambda_{DM}(y)$ is the seismic demand hazard differential with respect to DM and $G_{LS|DM}(y)$ is the probability of exceeding the limit state (LS) provided that DM is y (Baker and Cornell, 2006; Tothong and Cornell, 2007).

4 Modeling

4.1 Structural model

A four-floor structure with a concrete moment frame system was employed in this study. Figure 4 depicts the structure′s plan. The structure is symmetric in plan and elevation. Thus, nonlinear analyses can be performed on the structure on one of the lateral resisting frames, applying the P-Delta effects of the entire structure to the selected moment frame. The structural system selected to resist against the lateral loads is the perimeter moment frame. The lateral resisting systems in the x-direction of the plan are frames 1 and 5. The drifts of the entire structure in this direction are withstood by these two perimeter frames. Therefore, the other internal frames of the structure (known as the space frames or gravity frames) are only under the gravity loads. For the perimeter frames that resist lateral loads of the structure, the gravity loads that are directly withstood by the perimeter frames are different from the loads induced by the P-Delta effects. To consider the P-Delta effects, a pinned-end rigid column without lateral stiffness, known as the leaning column, is employed. The column is connected to the main structure by rigid beams (Fig. 5). To obtain the most accurate results in calculating structural collapse, the nonlinear concentrated plastic hinge model was used. Moreover, OpenSees software was employed for modeling and the nonlinear dynamic analyses. The pushover curve of a four-story frame with ID 1008 proposed by Haselton *et al.* (2008) was used to verify the model. Figure 6 shows the pushover curve of the modeled structure and the frame with ID 1008.

A total of 22 pairs of the far-fault records (a total of 44 records) proposed by FEMA-P695 (FEMA, 2009) were used for the IDA.

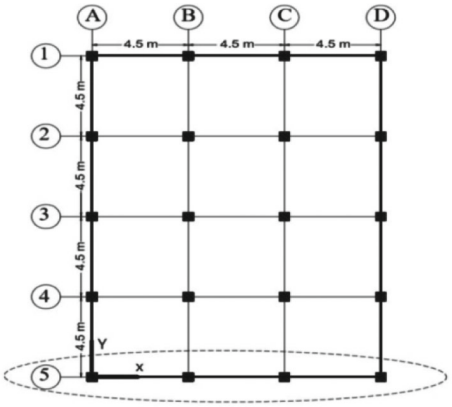

Fig. 4 Plan of the structure

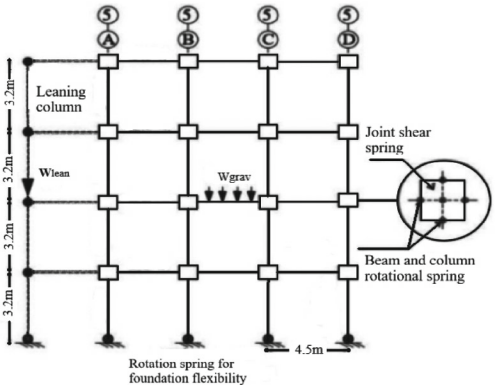

Fig. 5 Two-dimensional analytical moment frame model

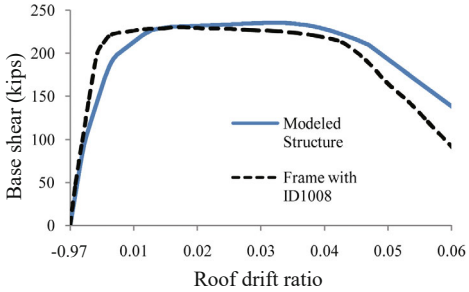

Fig. 6 Comparing the pushover curve of the modeled structure and the frame with ID 1008

4.2 Moment-rotation parameters of concentrated plastic hinge model

In this study, the concentrated plasticity model was employed for the beam and column components. The concentrated plastic hinge in the reinforced concrete structures was modeled using the tri-linear curve developed by Ibarra *et al*. (2005) (Fig. 7). The model involves the elastic area, post-yielding, and pre-capping area with positive slopes (K_s) and the post-capping area with a negative slope (K_c) and residual strength. The elastic area is defined by elastic stiffness (K_e) and yield moment (M_y). The post-yield and pre-capping area are defined by the plastic rotation capacity (θ_{cap}^{p}) and maximum moment or moment at the capping point (M_c). Moreover, the post-capping area is defined by the post-capping rotation capacity (θ_{pc}). Cycling stiffness and strength deterioration are calculated based on the energy dissipation capacity (λ). The plastic hinge parameters were calibrated by Haselton *et al.* (2008), for concrete components. The plastic hinge model is illustrated in Fig. 6 with the tri-linear curve.

4.3 IDA surves of structure

Incremental dynamic analysis (IDA) curves of the structure along with their 16th, 50th, and 84th percentiles are shown in Fig. 8.

4.4 Mean annual frequency of collapse limit state

The mean annual frequency (MAF) of the collapse limit state is calculated by extending Eq. (7) as

$$\lambda_{LS} = \int_{IM=0}^{IM=\infty} F(IM^{C}|IM) \cdot \left|\frac{d\lambda_{IM}}{dIM}\right| dIM \tag{7}$$

where $\left|\frac{d\lambda_{IM}}{dIM}\right|$ is the seismic hazard gradient and $F(IM^{C}|IM)$ is the cumulative probability function of the limit states. To calculate λ_{LS}, it is required to draw $F(IM^{C}|IM)$ for the collapse limit states, i.e., the fragility curve of the structure. Then, the above integration can be easily calculated using the numerical values of the site′s seismic hazard curve.

4.5 Seismic hazard curve

To calculate the seismic hazard gradient, the seismic hazard analysis of the site is required. Analyzing the seismic hazard for a site yields a uniform hazard spectrum with the return period of 475 years and 2,475 years. Then, the spectral accelerations of the return period of 475 and 2,475 years can be obtained for the site according to the fundamental period of the structure. The annual frequency of exceedance of the seismic intensity (i.e., the spectral acceleration in this study) is typically estimated by a linear relation in the logarithmic space as Eq. (8)

$$\lambda_{Sa} = k_0 (S_a)^{-k} \tag{8}$$

where λ_{Sa} is the reverse earthquake return period and S_a is the spectral acceleration corresponding to the uniform hazard spectrum at the return periods of 475 and 2,475 years. Moreover, k is the seismic hazard curve slope at the intended capacity and k_0 is the shape coefficient of the seismic hazard curve. To evaluate the seismic demand probability of the model, a site that was only affected by a point source and having the following properties was selected:

- Earthquake return period is 200 years;
- Magnitude of the event is 7.2;
- Nearest distance from the fault is 11 km;
- V_{s30} is 360 m/s for the site′s soil;
- Reverse type fault; and
- First mode period of the structure is 0.96.

The uniform hazard spectrum of the site at the return period of 475 years and 2,475 years is shown in Fig. 9.

Once the uniform hazard spectrum and fragility curves of the structure are obtained, the mean annual frequency of limit states can be calculated using Eq. (7). The mean annual frequencies of the collapse limit states are provided in Table 1.

Table 1 Seismic hazard parameters and mean annual frequency of collapse limit states

k_0	k	MAF ($\times 10^{-4}$)
0.000241	2.127	1.75

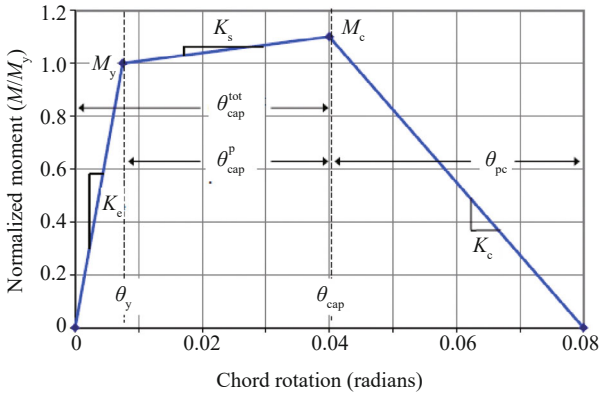

Fig. 7 Tri-linear backbone curve of the plastic hinge model

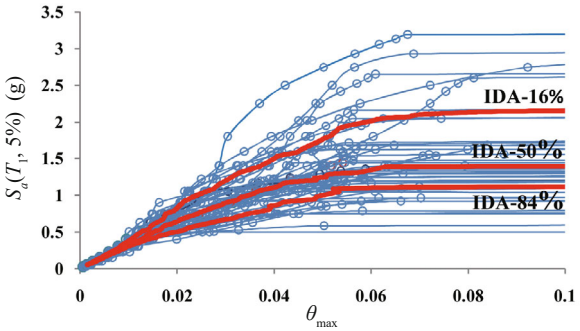

Fig. 8 IDA curves of the structure

5 Uncertainty analysis

5.1 Uncertainties

The concentrated plasticity model parameters introduced in Section 4.2 are considered as epistemic uncertainties. The mean values of the parameters are calculated using the equations proposed by Haselton *et al.* (2008). The parameters and their logarithmic standard deviations are as follows (Haselton *et al.*, 2008; Haselton and Deierlein, 2008):

(1) Effective initial stiffness, which is defined by the secant stiffness to 40% of yield force $\left(\frac{EI_{\text{stf}\,40}}{EI_{\text{g}}}\right)$, with a logarithmic standard deviation of 0.42 ($\sigma_{\text{LN}} = 0.42$);

(2) Bending (flexural) strength (M_{y}), which is calculated using the relation proposed by Panagiotakos and Fardis (2001), with a logarithmic standard deviation of 0.3 ($\sigma_{\text{LN}} = 0.3$);

(3) Plastic rotation capacity ($\theta_{\text{cap,pl}}$) with a logarithmic standard deviation of 0.63 ($\sigma_{\text{LN}} = 0.63$);

(4) Post-capping rotation capacity (θ_{pc}) with a logarithmic standard deviation of 0.86 ($\sigma_{\text{LN}} = 0.86$);

(5) Post-yield hardening stiffness or the ratio of the maximum moment and yield moment capacity ($M_{\text{c}}/M_{\text{y}}$) with a logarithmic standard deviation of 0.12 ($\sigma_{\text{LN}} = 0.12$); and

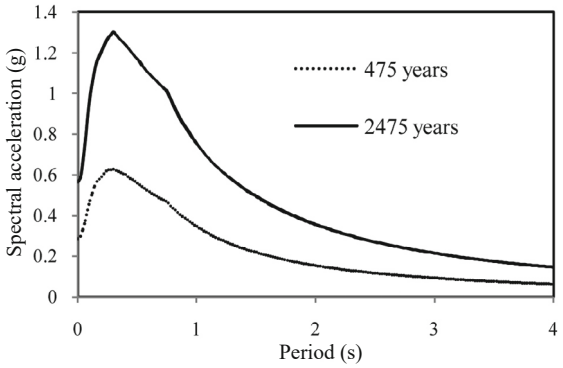

Fig. 9 Uniform hazard spectrum of the site at hazard level of 475 and 2,475 years

(6) Energy dissipation capacity for cyclic stiffness and strength deterioration (λ) with a logarithmic standard deviation of 0.64 ($\sigma_{\text{LN}} = 0.64$).

Six rotation-moment parameters of the concentrated plastic hinges were considered as epistemic uncertainties for the beam and column components – i.e., a total of 12 epistemic uncertainties (six for the beam and six for the column).

To evaluate the correlation of the model parameters in a component and between two structural components, the database built by Haselton *et al.* (2008) was employed. The correlation coefficients provided in Table 2 (Ugurhan *et al.*, 2014) were used to define correlations between the parameters of a structural component and correlation between the parameters of two structural components.

To incorporate the existing uncertainties in predicting the seismic intensity, an earthquake record is scaled such that it covers a wide range of intensities. Moreover, an acceptable number of earthquake records are used to consider the uncertainties in the frequency content and spectrum shape of earthquakes.

5.2 Sampling, simulation and satistical data production methods

Once the uncertainties of the beam and column components are known, independent and dependent random variables are produced to analyze the uncertainties using statistical measures, including mean, standard deviation, and uncertainties′ correlation.

Consider a multivariate random vector $\boldsymbol{X} = (X_1, X_2, \ldots, X_K)$ with normal distribution, mean vector μ_X, and covariance vector $\boldsymbol{C}_X$. Here, $\boldsymbol{X} = N(\boldsymbol{\mu}_X, \boldsymbol{C}_X)$, in which $\boldsymbol{\mu}_X = (\mu_1, \mu_2, \ldots, \mu_K)^{\text{T}}$ is a $K \times 1$ column vector (superscript T denotes the transpose of the matrix) and $\boldsymbol{C}_X$ is a $K \times K$ vector. The covariance matrix is a symmetric matrix in which $\sigma_{JK} = \sigma_{KJ}$, $J \neq K$, and $\sigma_{JK} = \text{Cov}(X_J, X_K)$.

A method to produce multivariate normal random variables is the square root algorithm. It functions by the orthogonal transformation using a covariance matrix

Table 2 Correlationsbetween parameters of a component and two structural components

		COMPONENT 1						COMPONENT 2					
		$\theta_{cap,pl1}$	θ_{pc1}	EI_{stf1}	M_{y1}	M_c/M_{y1}	γ_1	$\theta_{cap,pl2}$	θ_{pc2}	EI_{stf2}	M_{y2}	M_c/M_{y2}	γ_2
COMPONENT 1	$\theta_{cap,pl1}$	1	0.3	0	0.1	0.3	0.1	0.6	0.3	0	0.1	0.2	0
	θ_{pc1}		1	0.1	0.1	0.1	0.3		0.8	0.1	0.1	0.1	0.3
	$EIstf_1$			1	0.1	0	0			0.9	0.1	0.1	0
	M_{y1}				1	0.4	0.1				0.9	0.4	0.1
	M_c/M_{y1}		(sym.)			1	0.2		(sym.)			0.8	0.1
	γ_1						1						0.6
COMPONENT 2	$\theta_{cap,pl2}$							1	0.3	0	0.1	0.3	0.1
	θ_{pc2}								1	0.1	0.1	0.1	0.3
	EI_{stf2}				(symmetric)					1	0.1	0	0
	M_{y2}										1	0.4	0.1
	M_c/M_{y2}								(sym.)			1	0.2
	γ_2												1

$\boldsymbol{C}_X$ or correlation matrix $\boldsymbol{R}_X$. The square root algorithm decomposes the covariance and correlation matrices into $\boldsymbol{C}_X = \tilde{\boldsymbol{L}}\tilde{\boldsymbol{L}}'$ and $\boldsymbol{R}_X = \boldsymbol{L}\boldsymbol{L}'$, where $\boldsymbol{L}'$ is the transpose of $\boldsymbol{L}$, where $\boldsymbol{L}$ and $\tilde{\boldsymbol{L}}$ are the lower triangular matrices corresponding to the correlation matrix and covariance matrix, respectively.

In addition to symmetry, if $\boldsymbol{R}_X$ and $\boldsymbol{C}_X$ are positive finite matrices, the Cholesky decomposition is an effective approach to find $\boldsymbol{L}$ and $\tilde{\boldsymbol{L}}$. Using $\boldsymbol{L}$ or $\tilde{\boldsymbol{L}}$, the vector of multivariate normal random variables can be represented as Eq. (9)

$$\boldsymbol{X} = \boldsymbol{\mu}_X + \tilde{\boldsymbol{L}}\boldsymbol{Z}' \tag{9}$$

where $\boldsymbol{Z}'$ is a $K \times 1$ column vector of independent random variables with the mean of 0 and the standard deviation of 1 (the normal criterion variable).

Any typical matrix $\boldsymbol{A}$ can be decomposed into $\boldsymbol{A} = \boldsymbol{L}\boldsymbol{U}$, where $\boldsymbol{L}$ is a lower triangular matrix and $\boldsymbol{U}$ is an upper triangular matrix. If $\boldsymbol{A}$ is a symmetric positivefinite matrix, the relation can be represented as $\boldsymbol{A} = \boldsymbol{L}\boldsymbol{L}'$, where $\boldsymbol{U} = \boldsymbol{L}'$ (Tung and Yen, 2005).

According to Eq. (9) and the Cholesky decomposition method, dependent multivariate random variables are produced in the following steps:

1. Produce a lower triangular matrix of the correlation matrix or covariance matrix using the Cholesky method;
2. Produce independent random variables with a mean of 0 and a standard deviation of 1;
3. Use Eq. (9) to produce dependent random variables; and
4. Repeat steps 1 to 3 to generate the intended number of variables.

It is required to produce and simulate a sufficient number of samples for uncertainties to predict collapse fragility curves by considering epistemic uncertainties using RSM and ANN for the 12 introduced uncertainties (six belonging to the plastic hinge parameters of beams and six to the plastic hinge parameters of columns).

In this study, using the CCD method at a factorial level of 1/16, 281 samples were produced and simulated for the 12 epistemic uncertainties. The CCD samples were independent with a uniform distribution, the mean of 0, and the standard deviation of 1. To compare the results obtained from the CCD samples, 281 new independent samples were produced for the 12 uncertainties using the LHS method with considering the probability distribution of the uncertainties. The LHS independent samples also had a mean of 0 and a standard deviation of 1.

Let $\boldsymbol{x} = (x_1, x_2, x_3, \ldots, x_6)$ and $\boldsymbol{x} = (x_7, x_8, x_9, \ldots, x_{12})$ be the uncertainties of beam i and column j, respectively. Then, $\boldsymbol{x} = (x_1, x_2, x_3, \ldots, x_{12})$ is a set of dependent variables with the mean vector of $\boldsymbol{\mu}_x = (\mu_{x_1}, \mu_{x_2}, \mu_{x_3}, \ldots \mu_{x_{12}})$, standard deviation vector of $\boldsymbol{\sigma}_{\ln x} = (\sigma_{\ln x_1}, \sigma_{\ln x_2}, \sigma_{\ln x_3}, \ldots, \sigma_{\ln x_{12}})$, and covariance matrix of $\boldsymbol{\sigma}_{JK} = \mathrm{Cov}(x_J, x_K)$.

$\boldsymbol{Z}_1$ is a 281 × 12 matrix of the LHS independent normal variables produced with considering uncertainties probability distribution. $\boldsymbol{Z}_2$ is a 281 × 12 matrix of the CCD samples generated without considering uncertainties probability distribution. Hence, Eq. (11) is applied to produce dependent multivariate random variables as Eq. (10)

$$Y_k = \ln\boldsymbol{\mu}_X + \tilde{\boldsymbol{L}}\boldsymbol{Z}_k, \quad k = 1,\ 2 \tag{10}$$

where $\tilde{\boldsymbol{L}}$ is the lower triangular matrix corresponding to the covariance matrix obtained using the Cholesky decomposition.

To extend Eq. (10) to other beams and columns, the normalized matrix of the dependent random variables is generated using Eq. (11)

$$(X_k)_{ij} = \frac{(Y_k)_{ij} - \ln(\mu_{x_j})}{\sigma_{\ln x_j}} \quad (k = 1,\ 2;\ i = 1:281;\ j = 1:12) \tag{11}$$

Therefore, matrices $\boldsymbol{X}_1$ and $\boldsymbol{X}_2$ with the dimensions of 281 × 12 are composed of normalized dependent variables with the mean of 0 and the standard deviation of 1. Matrix $\boldsymbol{X}_1$ consists of 281 LHS simulations and matrix $\boldsymbol{X}_2$ includes 281 CCD simulations.

The uncertainties were normalized to reduce the dimensions of the problem, which reduced the number of the uncertainties to 12. Otherwise, there would have been six uncertainties for each beam or column, leading to a huge number of the total uncertainties by multiplying it by the number of the beams and columns of the structure.

6 Model outputs

6.1 Results of IDA analysis for different simulations

Matrices $\boldsymbol{X}_1$ and $\boldsymbol{X}_2$ were built using the normalized dependent variables to determine the input variables to perform nonlinear dynamic analyses on the 12 uncertainties of the structure (Eq. (11)). Then, to obtain the structural collapse responses, IDA was performed on each uncertainties simulation according to matrices $\boldsymbol{X}_1$ and $\boldsymbol{X}_2$ using the 44 introduced records and Hunt-Fill algorithm. Therefore, the mean collapse capacity (μ_{Sa} or $\mu_{\ln Sa}$), collapse standard deviation ($\sigma_{\ln Sa}$), and mean annual frequency (MAF) of collapse were obtained for each simulation.

Figure 10 represents the methodology of the present study to predict structural collapse responses by the RSM and ANN, with and without considering the probability distribution parameters of the uncertainties.

For both LHS and CCD methods, corresponding collapse responses were obtained and compared at statistical levels of 0 to 100%.

Therefore, according to Figs. 11 to 14, the correlation

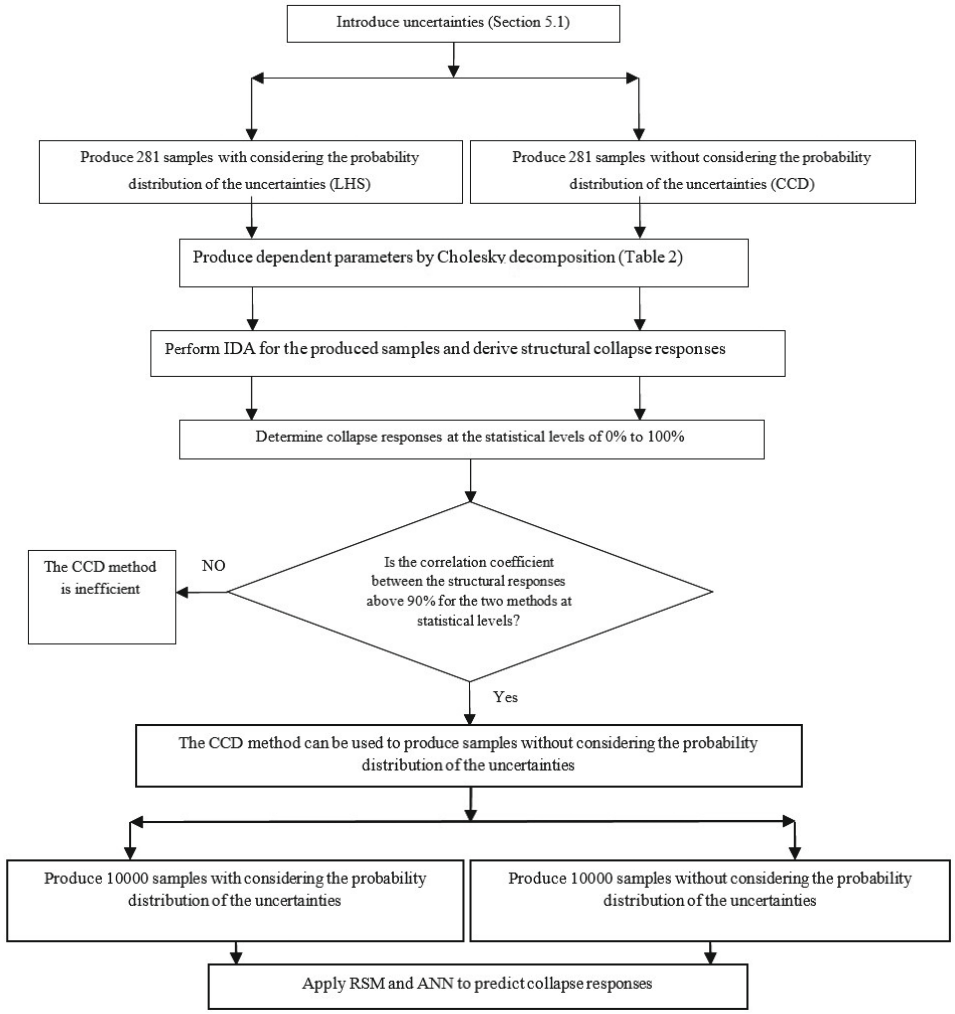

Fig. 10 Flowchart of the proposed methodology

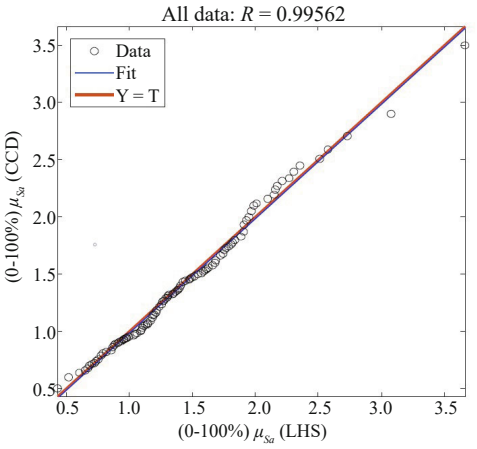

Fig. 11 Correlation coefficient between μ_{Sa} values at levels of 0 to 100% obtained from LHS and CCD methods

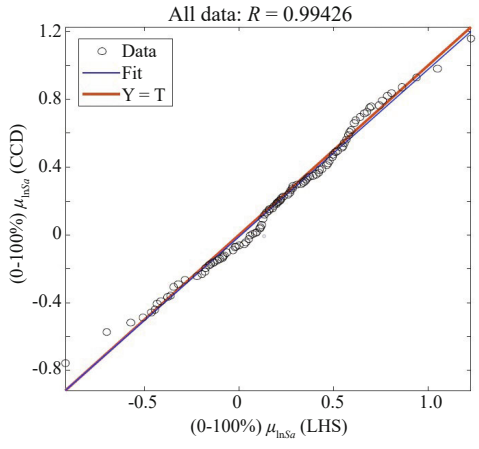

Fig. 12 Correlation coefficient between $\mu_{\ln Sa}$ values at levels of 0 to 100% obtained from LHS and CCD methods

coefficients between the collapse responses at statistical levels 0 to 100% for the LHS and CCD methods are 0.99562, 0.99426, 0.99261, and 0.97955 for μ_{Sa}, $\mu_{\ln Sa}$, $\sigma_{\ln Sa}$, and MAF, respectively.

Given the correlation coefficient (R) of above 0.98 between the collapse responses at the statistical levels of 0 to 100% for the two simulation methods, it was concluded that the CCD method can be used to produce samples and analyze uncertainties without considering the probability distribution parameters of the uncertainties.

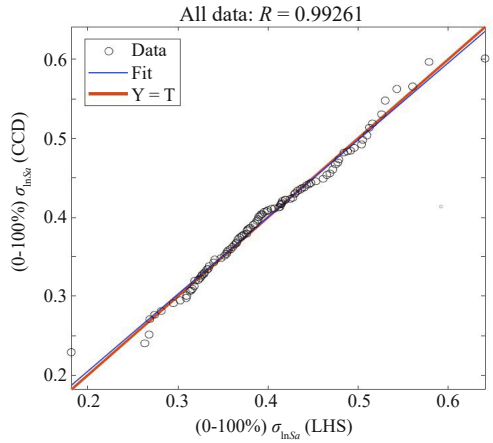

Fig. 13 Correlation coefficient between $\sigma_{\ln Sa}$ values at levels of 0 to 100% obtained from LHS and CCD methods

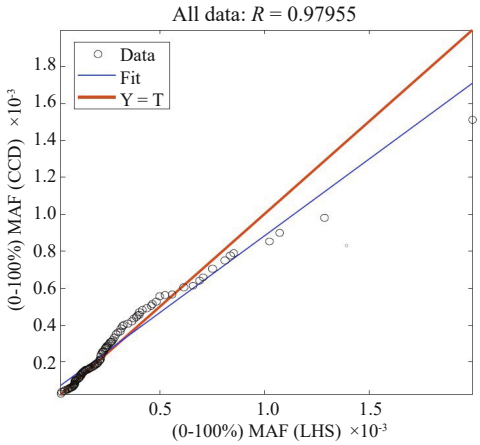

Fig. 14 Correlation coefficient between MAF values at levels of 0 to 100% obtained from LHS and CCD methods

6.2 Comparing different prediction methods

In this study, ANN and RSM were employed to predict collapse risk and collapse fragility curves by considering model uncertainties. The data of the input layer for 12 uncertainties consisted of 281 normalized independent variables generated by the LHS method ($\boldsymbol{Z}_1$) and 281 normalized independent variables generated by the CCD method ($\boldsymbol{Z}_2$). The target data were mean collapse capacity (μ_{Sa} or $\mu_{\ln Sa}$), collapse standard deviation ($\sigma_{\ln Sa}$), and mean annual frequency (MAF) obtained from IDA for the simulations. On the other hand, the output data in the ANN output layer were the predicted mean collapse capacity, collapse standard deviation, and mean annual frequency. To assess and compare the accuracy of the prediction methods, three criteria were employed: 1) correlation coefficient (R), 2) mean square error (MSE), and 3) root mean square error (RMSE), which are defined as Eqs. (12), (13) and (14), respectively. Moreover, the estimation error was calculated using Eq. (15):

$$R = \frac{\sum_{i=1}^{n}((y_{\text{obs}})_i - (\overline{y}_{\text{obs}})) \times ((y_{\text{est}})_i - (\overline{y}_{\text{est}}))}{\sqrt{\sum_{i=1}^{n}((y_{\text{obs}})_i - (\overline{y}_{\text{obs}}))^2 \sum_{i=1}^{n}((y_{\text{est}})_i - (\overline{y}_{\text{est}}))^2}} \tag{12}$$

$$\text{MSE} = \frac{\sum_{i=1}^{n}((y_{\text{est}})_i - (y_{\text{obs}})_i)^2}{n} \tag{13}$$

$$\text{RMSE} = \sqrt{\frac{\sum_{i=1}^{n}((y_{\text{est}})_i - (y_{\text{obs}})_i)^2}{n}} \tag{14}$$

Table 3 ANN structure

Topology	Transfer function	Training function
12-8-1	Tansing-Purelin	Levenberg-Marquardt

$$\text{Error} = \left(\frac{|\text{Estimated - Calculated}|}{\text{Calculated}}\right) \times 100 \tag{15}$$

where y_{obs} is the value obtained from IDA, $\overline{y}_{\text{obs}}$ is the mean value of the measures obtained from IDA, y_{est} is the predicted value, and $\overline{y}_{\text{est}}$ is the mean predicted value.

Table 3 provides the ANN structure. The number of neurons in the hidden layer of the network should be selected in a way that the network′s prediction error is minimized. The number of the hidden layers and neurons in the hidden layers was chosen to be 1 and 8, respectively.

The Tansig and Purline transfer functions were used in the hidden and output layers, respectively. The ANN was a feed-forward network with a back-propagation algorithm. Also, the Levenberg-Marquardt (LM) algorithm was applied to train the network. In this study, 70% of the data were used as training data, while the remaining 30% were employed as the test data.

Tables 4 and 5 provide the correlation coefficients (R) between the target data and the output data along with MSE and RMSE values for 281 LHS simulations and 281 CCD simulations for the training data, test data, and all data by the ANN.

Additionally, Table 6 represents the correlation coefficients (R) between the target data and the output data along with MSE and RMSE values for 281 LHS simulations and 281 CCD simulations for the all data by the RSM.

Three different tests were performed to compare the prediction methods to the IDA results for both LHS and

CCD simulations. In the first step, structural collapse responses were calculated by different methods while all the uncertainties were set to their mean values (Table 7). Then, collapse fragility curves were drawn (Fig. 15). It is seen in Fig. 16 that the maximum errors of μ_{Sa}, $\mu_{\ln Sa}$ and $\sigma_{\ln Sa}$ under RSM and ANN for the LHS method are about 6% and errors of MAF under RSM and ANN are 9% and 6%, respectively. At the same time, for CCD method, the maximum errors of μ_{Sa}, $\mu_{\ln Sa}$ and $\sigma_{\ln Sa}$ under RSM and ANN are about 6%, while the error of *MAF* under RSM and ANN is about 6%.

In the second step, S_a values corresponding to the collapse probability at the levels of 16%, 50%, and 84% were calculated (Table 8). The maximum error under RSM and ANN for the LHS and CCD methods is approximately 3.5%.

In the third test, structural collapse responses of LHS and CCD methods at levels of 16%, 50%, and 84% are

Table 4 Correlation coefficients (*R*), MSE, and RMSE of responses predicted by the ANN (LHS)

ANN (LHS)	Train data			Test data			All data		
	R	MSE	RMSE	*R*	MSE	RMSE	*R*	MSE	RMSE
μ_{Sa}	0.9984	0.00101	0.031772	0.9558	0.022543	0.15014	0.9877	0.007447	0.086293
$\mu_{\ln Sa}$	0.9984	0.00044651	0.021131	0.9588	0.013291	0.11529	0.9857	0.0042862	0.06547
$\sigma_{\ln Sa}$	0.9919	9.368×10^{-5}	0.0096787	0.7163	0.00334417	0.058666	0.9063	0.0010945	0.033082
MAF	0.998	4.625×10^{-10}	2.151×10^{-5}	0.8905	1.4566×10^{-8}	0.0001206	0.9768	4.679×10^{-9}	6.84×10^{-5}

Table 5 Correlation coefficients (*R*), MSE, and RMSE of responses predicted by the ANN (CCD)

ANN(CCD)	Train data			Test data			All data		
	R	MSE	RMSE	*R*	MSE	RMSE	*R*	MSE	RMSE
μ_{Sa}	0.9971	0.001837	0.042864	0.9402	0.035735	0.18904	0.9806	0.01197	0.10941
$\mu_{\ln Sa}$	0.9986	0.00041383	0.020343	0.9534	0.014478	0.12032	0.9846	0.0046181	0.067956
$\sigma_{\ln Sa}$	0.9858	0.00015166	0.012315	0.786	0.0025459	0.050457	0.9214	0.0008674	0.029451
MAF	0.9966	3.6976×10^{-10}	1.923×10^{-5}	0.9042	1.3469×10^{-8}	0.0001161	0.9632	4.286×10^{-9}	6.546×10^{-5}

Table 6 Correlation coefficients (*R*), MSE, and RMSE of responses predicted by the RSM

All data	RSM (LHS)			RSM (CCD)		
	R	MSE	RMSE	R	MSE	RMSE
μ_{Sa}	0.9875	0.007487	0.08653	0.9826	0.010572	0.10282
$\mu_{\ln Sa}$	0.9928	0.002148	0.04634	0.9882	0.0034365	0.05862
$\sigma_{\ln Sa}$	0.9139	0.0009104	0.03017	0.9173	0.00087735	0.02962
MAF	0.9875	2.426×10^{-9}	4.923×10^{-5}	0.9681	3.415×10^{-9}	5.844×10^{-5}

Table 7 Estimated collapse responses when all uncertainties are set to their mean values

	IDA	RSM (LHS)	ANN (LHS)	RSM (CCD)	ANN (CCD)
μ_{Sa}	1.504	1.493	1.524	1.499	1.54
$\mu_{\ln Sa}$	0.3242	0.3155	0.3123	0.3252	0.3434
$\sigma_{\ln Sa}$	0.422	0.3964	0.3996	0.3982	0.4112
MAF ($\times10^{-4}$)	1.75	1.59	1.65	1.64	1.86

Table 8 S_a values corresponding to the collapse probability at the levels of 16%, 50% and 84% when all uncertainties are set to their mean values

Collapse Probability	IDA	RSM (LHS)	ANN (LHS)	RSM (CCD)	ANN (CCD)
16%	0.91	0.93	0.92	0.93	0.94
50%	1.39	1.38	1.37	1.39	1.41
84%	2.11	2.04	2.04	2.06	2.12

provided in Tables 9 and 10 for IDA, RSM, and ANN results.

Then, 10,000 samples were produced with considering the probability distribution of the uncertainties, and 10,000 more samples were produced without considering the probability distribution of the uncertainties for the 12 epistemic uncertainties. However, since 6,600,000 nonlinear dynamic time-history analyses are required for each of the 10,000 simulations using 44 accelerogram records, and 15 incremental steps for each accelerogram using the Hunt-Fill algorithm, which is very time-consuming, the structural collapse responses are estimated only by the RSM and ANN approaches in a short time. Tables 9 and 10 provide the collapse responses at the levels of 16%, 50%, and 84%. Figures 17 to 20 show the predicted response errors from the IDA values for the 281 simulations.

- At levels of 16%, 50%, and 84%, the maximum μ_{Sa} errors for the LHS method and 281 simulations under RSM and ANN were 3.4% and 1.4%, respectively, while for 10,000 simulations under RSM and ANN, they were 2.5% and 1.3%, respectively.
- The maximum, μ_{Sa} errors for the CCD method and 281 simulations under RSM and ANN were 3.3% and 2.2%, respectively, while for 10,000 simulations under RSM and ANN, they were 5.3% and 1.8%, respectively.
- The maximum, $\mu_{\ln Sa}$ errors for the LHS method and 281 simulations under RSM and ANN were 6.8% and 3.3%, respectively, while for 10,000 simulations under RSM and ANN, they were 6.4% and 2.3%, respectively.
- The maximum, $\mu_{\ln Sa}$ errors for the CCD method and 281 simulations under RSM and ANN were 11% and 2.2%, respectively, while for 10,000 simulations under RSM and ANN, they were 16.7% and 15%, respectively.
- The maximum $\sigma_{\ln Sa}$ errors for the LHS method and 281 simulations under RSM and ANN were 3.2% and 2%, respectively, while for 10,000 simulations under RSM and ANN, they were 2.5% and 1.9%, respectively.
- The maximum $\sigma_{\ln Sa}$ errors for the CCD method and 281 simulations under RSM and ANN were 1.3%

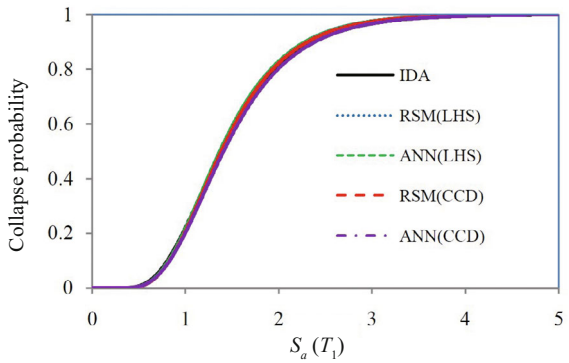

Fig. 15 Estimated collapse fragility curves when all uncertainties are set to their mean values

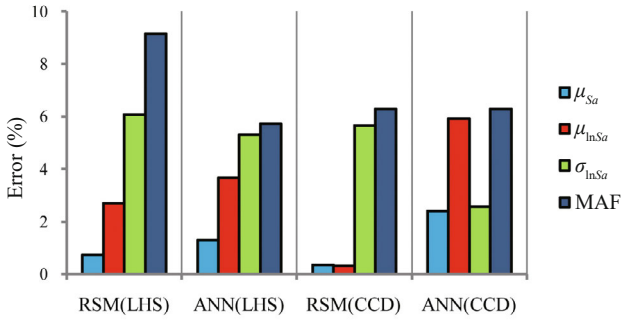

Fig. 16 μ_{Sa}, $\mu_{\ln Sa}$, $\sigma_{\ln Sa}$, and MAF errors when all uncertainties are set to their mean values

Table 9 Estimation of μ_{Sa}, $\mu_{\ln Sa}$, $\sigma_{\ln Sa}$, and MAF values at the levels of 16%, 50%, and 84% for the LHS method under RSM and ANN

LHS		IDA	RSM	ANN	RSM	ANN
Number of samples		281	281	281	10000	10000
μ_{Sa}	16%	0.889815	0.894587	0.901919	0.91179	0.89639
	50%	1.341208	1.387041	1.348254	1.3641	1.3547
	84%	1.946592	1.945388	1.951696	1.9411	1.9714
$\mu_{\ln Sa}$	16%	-0.17628	-0.16422	-0.18216	-0.16501	-0.1792
	50%	0.20706	0.220909	0.201245	0.21275	0.2119
	84%	0.584525	0.563205	0.582308	0.57535	0.5884
$\sigma_{\ln Sa}$	16%	0.324904	0.335367	0.31851	0.32905	0.3202
	50%	0.389693	0.39633	0.384123	0.39426	0.3971
	84%	0.477648	0.462676	0.482543	0.46554	0.4802
MAF	16%	9.293×10^{-5}	9.674×10^{-5}	0.0001015	9.579×10^{-5}	9.71×10^{-5}
	50%	0.0002146	0.0002123	0.0002109	0.0002069	0.0002163
	84%	0.0004638	0.0004525	0.0004768	0.0004534	0.0004767

Table 10 Estimation of μ_{Sa}, $\mu_{\ln Sa}$, $\sigma_{\ln Sa}$, and MAF values at the levels of 16%, 50%, and 84% for the CCD method under RSM and ANN

CCD		IDA	RSM	ANN	RSM	ANN
Number of samples		281	281	281	10000	10000
μ_{Sa}	16%	0.888668	0.859653	0.869548	0.84128	0.8723
	50%	1.321346	1.358001	1.329281	1.3292	1.3375
	84%	1.998194	1.98773	1.964654	1.9636	1.9867
$\mu_{\ln Sa}$	16%	-0.194743	-0.21268	-0.199084	-0.22725	-0.2239
	50%	0.195192	0.216703	0.193591	0.18263	0.2003
	84%	0.605813	0.590601	0.599812	0.57518	0.6052
$\sigma_{\ln Sa}$	16%	0.323115	0.327435	0.326781	0.32931	0.3121
	50%	0.400425	0.398295	0.398030	0.39665	0.3923
	84%	0.469604	0.465782	0.477167	0.46772	0.4813
MAF	16%	9.038×10^{-5}	8.336×10^{-5}	9.385×10^{-5}	9.556×10^{-5}	9.581×10^{-5}
	50%	0.0002149	0.0002517	0.0002328	0.0002301	0.0002287
	84%	0.0005166	0.0005373	0.0005483	0.0005201	0.0005012

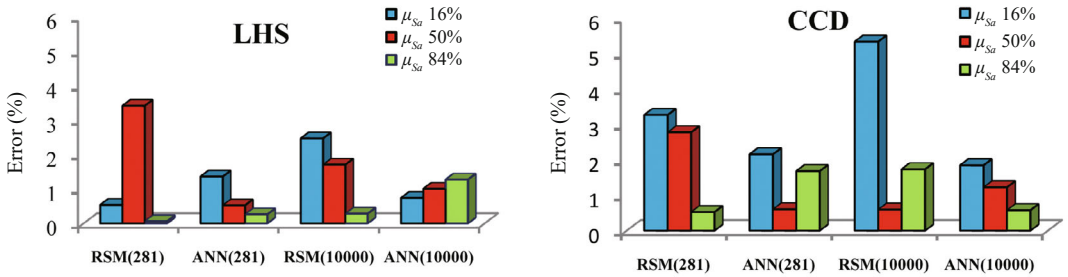

(a) LHS method (b) CCD method

Fig. 17 μ_{Sa} error at levels of 16%, 50%, and 84%

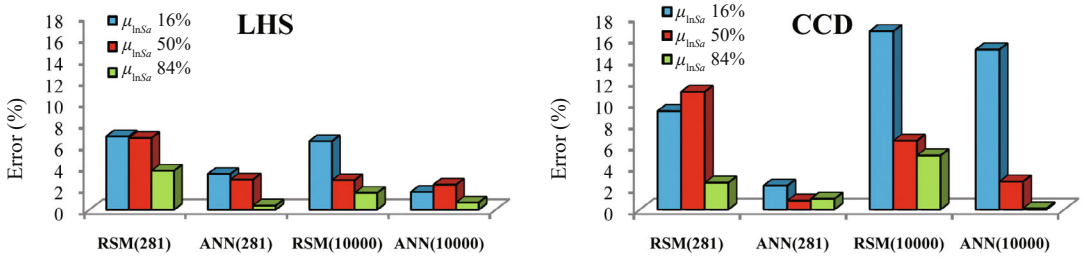

(a) LHS method (b) CCD method

Fig. 18 $\mu_{\ln Sa}$ error at levels of 16%, 50%, and 84%

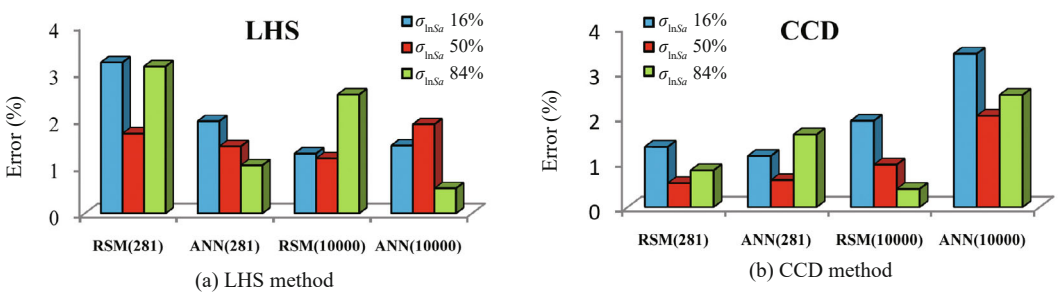

(a) LHS method (b) CCD method

Fig. 19 $\sigma_{\ln Sa}$ error at levels of 16%, 50%, and 84%

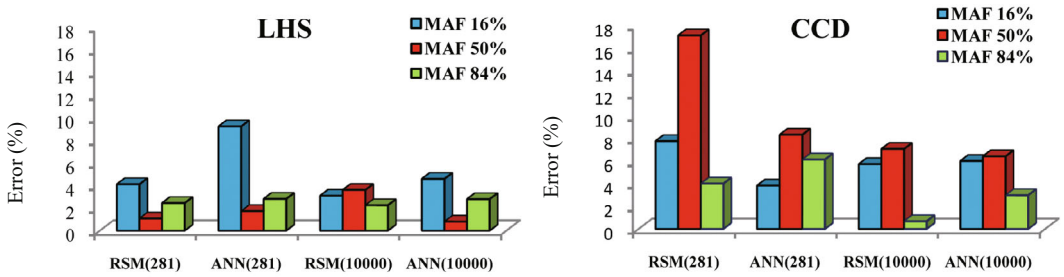

(a) LHS method (b) CCD method

Fig. 20 MAF error at of levels 16%, 50%, and 84%

and 1.6%, respectively, while for 10,000 simulations under RSM and ANN, they were 1.9% and 3.4%, respectively.

- The maximum MAF errors for the LHS method and 281 simulations under RSM and ANN were 4.1% and 9.2%, respectively, while for 10,000 simulations under RSM and ANN, they were 3.6% and 4.6%, respectively.
- The maximum MAF errors for the CCD method and 281 simulations under RSM and ANN were 17.1% and 8.3%, respectively, while for 10,000 simulations under RSM and ANN, they were 7.1% and 6.4%, respectively.

7 Summary and conclusions

This study was conducted to investigate collapse responses of a concrete moment frame structure by considering model uncertainties. The modeling uncertainties of collapse response evaluation were the parameters of the modified Ibarra-Medina-Krawinkler moment-rotation curve for beams and columns. For the uncertainty analysis, the correlations between the model parameters in a component and two structural components were considered. The Latin hypercube sampling (LHS) method was employed to produce independent random variables with considering the probability distribution of the uncertainties, while the central composite design (CCD) method was used to produce independent random variables without considering the probability distribution of the uncertainties. Next, the Cholesky decomposition was applied to produce dependent random variables for the two simulations. In the first step, 281 random variables were produced for the uncertainties using the LHS method by considering their correlation and IDA was performed with 44 far-fault accelerograms to determine the collapse response of the structure. For the 281 simulations using the 44 selected accelerograms 15 incremental steps for each accelerogram by the Hunt-Fill algorithm, a total of 185,460 nonlinear dynamic time-history analyses were performed. In the second step, 281 random variables were produced for the uncertainties using the CCD method by considering their correlations. For this purpose, 185,460 new dynamic nonlinear time history analyses were performed. Then, collapse responses were predicted for both simulation modes using RSM and ANN.

To compare the collapse responses of the two simulation modes, the collapse responses were obtained at statistical levels of 0 to 100%. The results revealed that the LHS and CCD correlation coefficients of μ_{Sa}, $\mu_{\ln Sa}$, $\sigma_{\ln Sa}$ and MAF at statistical levels of 0 to 100% are 0.99562, 0.99426, 0.99261, and 0.97955, respectively. Considering that the correlation coefficients were above 0.98 between the collapse responses at statistical levels of 0 to 100% in the two simulation methods, the CCD method can be employed to produce samples for uncertainty analysis and structural collapse response prediction without considering the probability distribution of uncertainties.

Three different tests were performed to compare the prediction methods to the IDA results for both LHS and CCD simulations. The results are as follows:

- When all the uncertainties are set to their mean values, under RSM and ANN, for the LHS method, the maximum errors of μ_{Sa}, $\mu_{\ln Sa}$ and $\sigma_{\ln Sa}$ were 6% and the maximum error of MAF was 9%. At the same time, for the CCD method, the maximum errors were 6% for μ_{Sa}, $\mu_{\ln Sa}$ and $\sigma_{\ln Sa}$ and 6% for MAF.
- The S_a errors at the collapse probability of 16%, 50%, and 84% for the LHS and CCD methods under RSM and ANN were about 3.5%.
- At levels of 16%, 50%, and 84%, for the LHS method and 281 simulations under RSM and ANN, the maximum μ_{Sa} errors were 3.4% and 1.4%, the maximum $\mu_{\ln Sa}$ errors were 6.8% and 3.3%, the maximum $\sigma_{\ln Sa}$ errors were 3.2% and 2%, and the maximum MAF errors were 4.1% and 9.2%, respectively, while for 10,000 simulations under RSM and ANN, the maximum μ_{Sa} errors were 2.5% and 1.3%, the maximum $\mu_{\ln Sa}$ errors were 6.4% and 2.3%, the maximum $\sigma_{\ln Sa}$ errors were 2.5% and 1.9%, and the maximum MAF errors were 3.6% and 4.6%, respectively.
- At levels of 16%, 50%, and 84%, for the CCD method and 281 simulations under RSM and ANN, the maximum μ_{Sa} errors were 3.3% and 2.2%, the maximum $\mu_{\ln Sa}$ errors were 11% and 2.2%, the maximum $\sigma_{\ln Sa}$ errors were 1.3% and 1.6%, and the maximum MAF errors

were 17% and 8.3%, respectively, while for 10,000 simulations under RSM and ANN, the maximum μ_{Sa} errors were 5.3% and 1.8%, the maximum $\mu_{\ln Sa}$ errors were 16.7% and 15%, the maximum $\sigma_{\ln Sa}$ errors were 1.9% and 3.4%, and the maximum *MAF* errors were 7.1% and 6.4%, respectively.

References

Anderson JA (1995), *An Introduction to Neural Networks*, MIT press.

Baker J and Cornell C (2006), "Vector-Valued Ground Motion Intensity Measures for Probabilistic Seismic Demand Analysis," *Report No. 150*, Pacific Earthquake Engineering Research Center, College of Engineering, University of California, Berkeley.

Beheshti-Aval SB, Khojastehfar E, Noori M and Zolfaghari M (2015), "A Comprehensive Collapse Fragility Assessment of Moment Resisting Steel Frames Considering Various Sources of Uncertainties," *Canadian Journal of Civil Engineering*, **43**(2): 118–131.

Borekci M, Kirçil M and Ekiz I (2014), "Collapse Period of Degrading SDOF Systems," *Earthquake Engineering and Engineering Vibration*, **13**(4): 681–694.

Bucher C and Most T (2008), "A Comparison of Approximate Response Functions in Structural Reliability Analysis," *Probabilistic Engineering Mechanics*, **23**(2-3): 154–163.

Buratti N, Ferracuti B and Savoia M (2010), "Response Surface with Random Factors for Seismic Fragility of Reinforced Concrete Frames," *Structural Safety*, **32**(1): 42–51.

Der Kiureghian A and Ditlevsen O (2009), "Aleatory or epistemic? Does it matter?" *Structural Safety*, **31**(2): 105–112.

Fattahi F and Gholizadeh S (2019), "Seismic Fragility Assessment of Optimally Designed Steel Moment Frames," *Engineering Structures*, **179**: 37–51.

Federal Emergency Management Agency (2000), *FEMA 350*, *Recommended Seismic Design Criteria for New Steel Moment-Frame Buildings*, SAC joint Venture, Washington, DC.

Federal Emergency Management Agency (2009), *FEMA P-695*, *Quantification of Buildings Seismic Performance Factors*, Washington, DC.

Gholizadeh S and Aligholizadeh V (2019), "Reliability-Based Optimum Seismic Design of RC Frames by a Metamodel and Metaheuristics," *The Structural Design of Tall and Special Buildings*, **28**(1): e1552 (19 Pages).

Gholizadeh S and Mohammadi M (2016), "Reliability-Based Seismic Optimization of Steel Frames by Metaheuristics and Neural Networks," *ASCE-ASME Journal of Risk and Uncertainty in Engineering Systems*, *Part A: Civil Engineering*, **3**(1): 04016013 (11 Pages).

Gomes HM and Awruch AM (2004), "Comparison of Response Surface and Neural Network with Other Methods for Structural Reliability Analysis," *Structural Safety*, **26**(1): 49–67.

Haselton CB and Deierlein GG (2008), "Assessing Seismic Collapse Safety of Modern Reinforced Concrete Moment-Frame Buildings," *Report No. PEER 2007/08*, Pacific Earthquake Engineering Research Center, College of Engineering, University of California, Berkeley.

Haselton CB, Liel AB, Lange ST and Deierlein GG (2008), "Beam-Column Element Model Calibrated for Predicting Flexural Response Leading to Global Collapse of RC Frame Buildings," *Report No. PEER 2007/03*, Pacific Earthquake Engineering Research Center, College of Engineering, University of California, Berkeley.

Hassanzadeh A and Gholizadeh S (2019), "Collapse-Performance-Aided Design Optimization of Steel Concentrically Braced Frames," *Engineering Structures*, **197**: 109411 (15 Pages).

Ibarra LF and Krawinkler H (2005), "Global Collapse of Frame Structures Under Seismic Excitations,"*Report No.152*, Pacific Earthquake Engineering Research Center Berkeley, CA.

Ibarra LF, Medina RA and Krawinkler H (2005), "Hysteretic Models that Incorporate Strength and Stiffness Deterioration,"*Earthquake Engineering and Structural Dynamics*, **34**(12): 1489–1511.

Karimi Ghaleh Jough F and Beheshti Aval S (2018), "Uncertainty Analysis Through Development of Seismic Fragility Curve for an SMRF Structure Using an Adaptive Neuro-Fuzzy Inference System Based on Fuzzy C-Means Algorithm," *Scientia Iranica*, **25**(6): 2938–2953.

Karimi Ghaleh Jough F and Şensoy S (2016), "Prediction of Seismic Collapse Risk of Steel Moment Frame Mid-Rise Structures by Meta-Heuristic Algorithms," *Earthquake Engineering and Engineering Vibration*, **15**(4): 743–757.

Karimi Ghaleh Jough F and Şensoy S (2020), "Steel Moment-Resisting Frame Reliability via the Interval Analysis by FCM-PSO Approach considering Various Uncertainties," *Journal of Earthquake Engineering*, **24**(1): 109–128.

Khojastehfar E, Beheshti-Aval SB, Zolfaghari MR and Nasrollahzade K (2014), "Collapse Fragility Curve Development Using Monte Carlo Simulation and Artificial Neural Network," *Proceedings of the Institution of Mechanical Engineers, Part O: Journal of Risk and Reliability*, **228**(3): 301–312.

Li X (1996), "Simultaneous Approximations of Multivariate Functions and Their Derivatives by Neural Networks with One Hidden Layer," *Neurocomputing*, **12**(4): 327–343.

Liel AB, Haselton CB, Deierlein GG and Baker JW (2009), "Incorporating Modeling Uncertainties in the

Assessment of Seismic Collapse Risk of Buildings," *Structural Safety*, **31**(2): 197–211.

Lignos DG and Krawinkler H (2010), "Deterioration Modeling of Steel Components in Support of Collapse Prediction of Steel Moment Frames Under Earthquake Loading," *Journal of Structural Engineering*, **137**(11): 1291–1302.

Myers RH, Montgomery DC and Anderson-Cook CM (2009), -*Response Surface Methodology: Process and Product Optimization Using Designed Experiments*, John Wiley & Sons., New York.

Palanci M (2019), "Fuzzy Rule Based Seismic Risk Assessment of One-Story Precast Industrial Buildings," *Earthquake Engineering and Engineering Vibration*, **18**(3): 631–648.

Panagiotakos TB and Fardis MN (2001), "Deformations of Reinforced Concrete Members at Yielding and Ultimate," *Structural Journal*, **98**(2): 135–148.

Park J and Towashiraporn P (2014), "Rapid Seismic Damage Assessment of Railway Bridges Using the Response-Surface Statistical Model," *Structural Safety*, **47**: 1–12.

Tothong P and Cornell CA (2007), "Probabilistic Seismic Demand Analysis Using Advanced Ground Motion Intensity Measures, Attenuation Relationships, and Near-Fault Effects," *Report No. PEER 2006/11*, Pacific Earthquake Engineering Research Center, College of Engineering, University of California, Berkeley.

Tung Y-K and Yen BC (2005), *Hydrosystems Engineering Uncertainty Analysis*, McGraw-Hill New York.

Ugurhan B, Baker J and Deierlein G (2014), "Uncertainty Estimation in Seismic Collapse Assessment of Modern Reinforced Concrete Moment Frame Buildings,"*Proceedings of the 10th National Conference in Earthquake Engineering,* Anchorage, Alaska.

Vamvatsikos D and Cornell CA (2002), "Incremental Dynamic Analysis," *Earthquake Engineering & Structural Dynamics*, **31**(3): 491–514.

Vamvatsikos D and Cornell CA (2004), "Applied Incremental Dynamic Analysis," *Earthquake Spectra*, **20**(2): 523–553.

Zareian F and Krawinkler H (2007), "Assessment of Probability of Collapse and Design for Collapse Safety," *Earthquake Engineering & Structural Dynamics*, **36**(13): 1901–1914.

Zareian F, Krawinkler H, Ibarra L and Lignos D (2010), "Basic Concepts and Performance Measures in Prediction of Collapse of Buildings under Earthquake Ground Motions," *The Structural Design of Tall and Special Buildings*, **19**(1-2): 167–181.

Zhang D, Han X, Jiang C, Liu J and Li Q (2017), "Time-Dependent Reliability Analysis Through Response Surface Method," *Journal of Mechanical Design*, **139**(4): 041404 (12 pages).